

Supercontinuum generation of ultrashort laser pulses in air at different central wavelengths

Stefan Skupin, Luc Bergé

Département de Physique Théorique et Appliquée, CEA/DAM Ile de France, B.P. 12, 91680 Bruyères-le-Châtel, France

Abstract

Supercontinuum generation by femtosecond filaments in air is investigated for different laser wavelengths ranging from ultraviolet to infrared. Particular attention is paid on the role of third-harmonic generation and temporal steepening effects, which enlarge the blue part of the spectrum. A unidirectional pulse propagation model and nonlinear evolution equations are numerically integrated and their results are compared. Apart from the choice of the central wavelength, we emphasize the importance of the saturation intensity reached by self-guided pulses, together with their temporal duration and propagation length as key players acting on both supercontinuum generation of the pump wave and emergence of the third harmonics. Maximal broadening is observed for large wavelengths and long filamentation ranges.

Key words: Supercontinuum Generation, Femtosecond Filaments, Nonlinear Schrödinger Equation, Self-phase Modulation

PACS: 42.65.Tg, 52.38.Hb, 42.65.Jx, 42.68.Ay

1. Introduction

Third harmonic (TH) generation and supercontinuum (SC) emission are two phenomena which have attracted broad interest in the past years [1,2,3,4,5]. An evident reason is their direct application in atmospheric remote sensing measurements based on LIDAR (Light Detection And Ranging) femtosecond laser setups [6]. In this context, spectral broadening originates from complex mechanisms that drive the long-range propagation of ultrashort pulses, when they form narrow filaments in optically-transparent media.

The physics of isolated femtosecond filaments in air is nowadays rather well understood (see, e.g., [7] and references therein). It involves the competition between Kerr self-focusing and plasma defocusing, triggered whenever the input pulse power exceeds the critical power for self-focusing $P_{\text{cr}} \simeq \lambda_0^2 / (2\pi n_0 n_2)$. Here, λ_0 is the central laser wavelength, $n_0 = 1$ and n_2 are the linear and nonlinear refraction indices in air, respectively. For high enough powers, multiple filaments nucleated after an early stage of modulational instability have also been widely investigated [7,8,9]. They produce spectral patterns mostly analogous to those generated by a single filament, as filamentary cells emerge

in phase from the background field and possess the same phase link [10]. By comparing Terawatt (TW) multifilamented beams with Gigawatt (GW) single filaments in air, this property was again verified in the UV-visible region (230-500 nm), where femtosecond self-focusing pulses centered at 800 nm generically produce a tremendous plateau of wavelengths [11,12,13].

This latter phenomenon has recently become a subject of inspiration for several researchers. Two scenarios have been proposed for justifying the build-up of new wavelengths in the UV-visible range. On the one hand, temporal steepening phenomena undergone by the pump were shown to deeply modify the filament spectrum [14]. Full chromatic dispersion included in the optical field wave number $k(\omega)$ affects both the diffraction operator and the nonlinearities. This induces shock-like dynamics at the back edge of the pulse through space-time focusing and self-steepening effects, which strongly "blueshift" the spectra. On the other hand, spectral broadening becomes enhanced by harmonic generation. The coupling of TH with an infrared (IR) pump produces a "two-colored" filament from pump intensities above 10 TW/cm² [15,16,17]. The amount of pump energy transferred into TH radiation depends on the linear wave vector mismatch parameter $\Delta k = [3k(\omega) - k(3\omega)]^{-1}$ fixing the coherence length $L_c = \pi/|\Delta k|$. The smaller the coherence length, the weaker TH fields. Along meter-range

Email addresses: stefan.skupin@cea.fr (Stefan Skupin), luc.berge@cea.fr (Luc Bergé).

distances, the TH component can stabilize the pump wave with about 0.5% conversion efficiency [13]. Experimental and numerical data reported ring structures embarking most of the TH energy and having a half-divergence angle of about 0.5 mrad [18]. This process contributes to create a continuous spectral band of UV-visible wavelengths [11,13,19].

Resembling spectral dynamics have also been reported from 1-mJ infrared pulses propagating in argon at atmospheric pressure, after subsequent compression by chirped mirrors [20]. Simulations of these experiments [21], discarding TH emission, revealed that temporal gradients inherent to the steepening operators are sufficient to amplify UV shifts and cover the TH bandwidth down to 250 and 210 nm for initial pulse durations of 10 and 6 fs, respectively. Very recently, numerical simulations [22] refound this tendency for atmospheric propagation, i.e., TH generation, while it affects the pump dynamics to some extent over long ranges, does not change significantly SC spectra, whose variations are mostly induced by the fundamental field in air.

Despite these last results, we are still missing a detailed understanding of the key parameters which are supposed to drive SC generation. A first important parameter is, of course, the laser wavelength itself: How does the supercontinuum evolve when λ_0 is varied? This question was addressed in Ref. [11] for various laser wavelengths, at which some spectral components were seen to merge. However, the model used a two-envelope approximation (for the pump and TH fields, separately). As emphasized in [22], splitting into TH and SC pump within envelopes becomes problematic when their respective spectra overlap inside a wide frequency interval where the basic validity condition $\Delta\omega_j/\omega_j \ll 1$ ($j = \omega, 3\omega$) may no longer be fulfilled. Actually, TH radiation produced through the nonlinear polarization needs to be described self-consistently from a single equation governing the total real optical field. This model was missing in Refs. [13,19], which made the role of TH overestimated in the white light emission. Another important parameter is the length of the self-guiding range: Successive cycles of focusing and defocusing events promote the creation of shorter peaks in the pulse temporal profile and lead to a maximal extension of the spectrum. A third potential player is the input pulse duration. In [21], this was shown to affect the spectra in noble gases for pulses containing a few optical cycles mainly. Clearing this aspect requires several simulations using distinct pulse durations and exploiting different propagation ranges. In connection, we demonstrate that spectral enlargements are directly linked to the level of maximum intensity: Steepening operators as well as TH radiation broaden all the more the spectra as the intensity in the filament is high.

The paper is organized as follows: Sec. 2 presents the model equations, namely, a unidirectional propagation equation for the total electric field that generates higher-order harmonics (mostly TH) through Kerr nonlinearities. Results from this equation will be compared with those inferred from the "standard" nonlinear evolution equation

(NEE) for the pump wave. The major difference between these two models lies in the production of the TH field and its coupling with the pump wave. Sec. 3 is devoted to the long-range propagation of 127-fs pulses in air described by the previous models. Emphasis is put on the influence of the central wavelength λ_0 (248, 800, 1550 nm). We discuss spectral modifications versus the height of I_{\max} , the input duration, together with the temporal steepening dynamics and merging between TH and pump spectral bands. Sec. 4 revisits SC for short-range (focused) propagations. It is shown that I_{\max} becomes closer to analytical evaluations when the beam develops few focusing/defocusing cycles. In this configuration, a lesser broadening may be achieved. Sec. 5 finally summarizes the generic features resulting from our analysis.

2. Models for pulse propagation and underlying physics

Our unidirectional pulse propagation equation (UPPE) assumes scalar and radially-symmetric approximations. It also supposes negligible backscattering. These hypotheses hold as long as the beam keeps transverse extensions larger than the central laser wavelength and as the nonlinear responses (together with their longitudinal variations) are small compared with the linear refraction index. Straight-forward manipulations of Maxwell equations allow us to establish the equation for the spectral amplitude of the optical electric field in the forward direction as [7]

$$\partial_z \hat{E} = \frac{i}{2k(\omega)} \nabla_{\perp}^2 \hat{E} + ik(\omega) \hat{E} + \frac{i\mu_0\omega^2}{2k(\omega)} \hat{\mathcal{F}}_{\text{NL}}, \quad (1)$$

where $\hat{E}(r, z, \omega) = (2\pi)^{-1} \int E(r, z, t) e^{i\omega t} dt$ is the Fourier transform of the forward electric field component, z is the propagation variable, $\nabla_{\perp}^2 = r^{-1} \partial_r r \partial_r$ ($r \equiv \sqrt{x^2 + y^2}$) is the diffraction operator, $\mu_0\epsilon_0 = 1/c^2$, $k(\omega) = \sqrt{1 + \chi^{(1)}(\omega)}\omega/c$ is the wavenumber of the optical field depending on the linear susceptibility tensor $\chi^{(1)}(\omega)$ defined at frequency ω . In Eq. (1), $\hat{\mathcal{F}}_{\text{NL}} \equiv \hat{P}_{\text{NL}} + i\hat{J}/\omega$ is the Fourier transform of the nonlinearities that include the nonlinear optical polarization P_{NL} and the current density J created by charged particles. Eq. (1) restores the earlier UPPE formulation proposed by Kolesik *et al.* [23] in the limit $k_{\perp}^2/k^2(\omega) \ll 1$ ($k_{\perp}^2 = k_x^2 + k_y^2$).

For practical use, it is convenient to introduce the complex version of the electric field

$$E = \sqrt{c_1}(\mathcal{E} + \mathcal{E}^*), \quad \mathcal{E} = \frac{1}{\sqrt{c_1}} \int \Theta(\omega) \hat{E} e^{-i\omega t} d\omega, \quad (2)$$

where $c_1 \equiv \omega_0\mu_0/2k_0$ employs the central wavenumber and frequency of the pump wave ($k_0 \equiv n_0\omega_0/c$) and $\Theta(x)$ denotes the Heaviside function. Because \mathcal{E} satisfies $\widehat{\mathcal{E}^*}(\omega) = \hat{\mathcal{E}}(-\omega)^*$ (* means complex conjugate), it is then sufficient to treat the UPPE model (1) in the frequency domain $\omega > 0$ only. The field intensity can be defined by E^2 averaged

over an optical period at least. Expressed in W/cm^2 , it is simply given by the classical relation $I = |\mathcal{E}|^2$.

Concerning the nonlinearities, we assume a linearly polarized field. We consider a cubic susceptibility tensor $\chi^{(3)}$ keeping a constant value around ω_0 , so that P_{NL} contains the instantaneous cubic polarization expressed as $P^{(3)}(\mathbf{r}, t) = \epsilon_0 \chi_{\omega_0}^{(3)} E^3$. In addition, the phenomenon of Raman scattering comes into play when the laser field interacts with anisotropic molecules, in which vibrational and rotational states are excited. Depending on the transition frequency Ω_{13} in three-level molecular systems and related dipole matrix element μ [24], the Raman response takes the form

$$P_{\text{Raman}} = \frac{2\chi^{(1)}\mu^2}{\Omega_{31}\hbar^2} \int_{-\infty}^t e^{-\frac{t-t'}{\tau_2}} \sin\left(\frac{t-t'}{\tau_1}\right) E^2(t') dt' \times E, \quad (3)$$

where $\tau_1 = 1/\omega_R$ is the inverse of the fundamental rotational frequency and τ_2 is the dipole dephasing time. Expressed in terms of the rescaled complex field \mathcal{E} [Eq. (2)] and with appropriate normalizations [25], Eq. (3) completes the cubic polarization as

$$P_{\text{NL}} = 2n_0 n_2 \epsilon_0 \sqrt{c_1} \int_{-\infty}^{+\infty} \bar{R}(t-t') |\mathcal{E}(t')|^2 dt' \mathcal{E} + 2n_0 n_2 \epsilon_0 \sqrt{c_1} (1 - x_K) \mathcal{E}^3 / 3 + c.c., \quad (4a)$$

$$\bar{R}(t) = (1 - x_K) \delta(t) + x_K \Theta(t) h(t), \quad (4b)$$

$$h(t) = \frac{\tau_1^2 + \tau_2^2}{\tau_1 \tau_2^2} e^{-t/\tau_2} \sin(t/\tau_1), \quad (4c)$$

where $n_2 = 3\chi_{\omega_0}^{(3)}/(4n_0^2 c \epsilon_0)$ is the Kerr nonlinear index. Expression (4a) possesses both retarded and instantaneous components in the ratio x_K . The instantaneous part $\sim \delta(t)$ of Eq. (4b) describes the response from the bound electrons. The retarded part $\sim h(t)$ accounts for the Raman contribution, in which fast oscillations in E^2 give negligible contributions, as $\tau_1 \sim \tau_2 \sim 70$ fs are assumed to exceed the optical period $\sim \omega_0^{-1}$.

When free electrons are created, they induce a current density $J = q_e \rho v_e$, which depends on the electron charge q_e , the electron density ρ and the electron velocity v_e . J is computed from fluid equations involving external plasma sources and the electron collision frequency ν_e . At moderate intensities ($< 10^{15} \text{ W}/\text{cm}^2$), the current density obeys

$$\partial_t J + \nu_e J = \frac{q_e^2 \rho}{m_e} E. \quad (5)$$

Assuming electrons born at rest, the growth of the electron density is only governed by external source terms, i.e.,

$$\partial_t \rho = W(I)(\rho_{\text{nt}} - \rho) + \frac{\sigma}{U_i} \rho I, \quad (6)$$

that include photo-ionization processes with rate $W(I)$ and collisional ionization with cross-section

$$\sigma(\omega) = \frac{q_e^2}{m_e \epsilon_0 n_0 c \nu_e (1 + \omega^2/\nu_e^2)}. \quad (7)$$

Here, ρ_{nt} and U_i are the density of neutral species and the ionization potential, respectively. Electron recombination

in gases is efficient over long (ns) time scales, and therefore we omit it. In Eq. (6), the rate for photo-ionization $W(I)$ follows from the Perelomov, Popov and Terent'ev (PPT)'s theory [26] incorporating Ammosov, Delone and Krainov (ADK) coefficients [27] (see also Ref. [28]). Optical field ionization theories stress two major limits bounded by the Keldysh parameter,

$$\gamma = \omega_0 \frac{\sqrt{2m_e U_i}}{|q_e| E_p}, \quad (8)$$

namely, the limit for Multi-Photon Ionization (MPI, $\gamma \gg 1$) concerned with rather low intensities and the tunnel limit ($\gamma \ll 1$) concerned with high intensities, from which the Coulomb barrier becomes low enough to let the electron tunnel out. Here, E_p denotes the peak optical amplitude. For laser intensities $I = |\mathcal{E}|^2 < 10^{13} - 10^{14} \text{ W}/\text{cm}^2$, MPI characterized by the limit

$$W(I) \rightarrow W_{\text{MPI}} = \sigma_K I^K \quad (9)$$

dominates, where $K = \text{mod}(U_i/\hbar\omega_0) + 1$ is the number of photons necessary to liberate one electron. The level of clamped intensity, I_{max} , depends on the selected ionization rate.

Energy lost by the pulse through single ionization processes is determined by a local version of the Poynting theorem, yielding the loss current J_{loss} , such that $J_{\text{loss}} \cdot E = U_i W(I)(\rho_{\text{nt}} - \rho)$. As a result, our UPPE model reads in Fourier space as

$$\begin{aligned} \frac{\partial}{\partial z} \hat{\mathcal{E}} = & \left[\frac{i}{2k(\omega)} \nabla_{\perp}^2 + ik(\omega) \right] \hat{\mathcal{E}} + \frac{i\mu_0 \omega^2}{2k(\omega) \sqrt{c_1}} \Theta(\omega) \hat{P}_{\text{NL}} \\ & - \frac{ik_0^2 \Theta(\omega)}{2\epsilon(\omega_0) k(\omega) (1 + \frac{\nu_e^2}{\omega^2})} \left(\frac{\rho \hat{\mathcal{E}}}{\rho_c} \right) - \frac{\Theta(\omega)}{2} \sqrt{\frac{\epsilon(\omega_0)}{\epsilon(\omega)}} \mathcal{L}(\omega), \end{aligned} \quad (10)$$

where

$$\mathcal{L}(\omega) = \frac{U_i}{2\pi} \int \mathcal{E} \left[\frac{W(I)}{I} (\rho_{\text{nt}} - \rho) + \frac{\sigma(\omega)}{U_i} \rho \right] e^{i\omega t} dt. \quad (11)$$

In Eq. (10), P_{NL} and the expression containing the electron density $\rho(\mathbf{r}, t)$ [Eq. (6)] must be transformed to Fourier space, from which we retain only positive frequencies for the symmetry reasons given above.

Alternatively, when a central frequency ω_0 is imposed, Eq. (1) restitutes the Nonlinear Envelope Equation (NEE), earlier derived by Brabec and Krausz [29]. We can make use of the Taylor expansion

$$k(\omega) = k_0 + k' \bar{\omega} + \hat{\mathcal{D}}, \quad \hat{\mathcal{D}} \equiv \sum_{n \geq 2}^{+\infty} \frac{k^{(n)}}{n!} \bar{\omega}^n, \quad (12)$$

where $\bar{\omega} = \omega - \omega_0$, $k' = \partial k / \partial \omega|_{\omega=\omega_0}$, $k^{(n)} = \partial^n k / \partial \omega^n|_{\omega=\omega_0}$, and take the inverse Fourier transform of Eq. (1) in which terms with $k(\omega)$ in their denominator are expanded up to first order in $\bar{\omega}$ only. After introducing the complex-field representation $\mathcal{E} = U e^{ik_0 z - i\omega_0 t}$, the new time variable $t \rightarrow t - z/v_g$ can be utilized to replace the pulse into the

frame moving with the group velocity $v_g = k'^{-1}$. Furthermore assuming $\nu_e^2/\omega_0^2 \ll 1$, $\sqrt{\epsilon(\omega_0)/\epsilon(\omega)} \approx 1$ and ignoring the TH component, the nonlinear envelope equation for the forward pump envelope U expands as follows:

$$\begin{aligned} \frac{\partial}{\partial z} U = & \frac{i}{2k_0} T^{-1} \nabla_{\perp}^2 U + i \mathcal{D} U + i \frac{\omega_0}{c} n_2 T \times \\ & \left[(1 - x_K) |U|^2 + x_K \int_{-\infty}^t h(t-t') |U(t')|^2 dt' \right] U \\ & - i \frac{k_0}{2n_0^2 \rho_c} T^{-1} \rho U - \frac{\sigma}{2} \rho U - (\rho_{nt} - \rho) \frac{U_i W(I)}{2|U|^2} U, \end{aligned} \quad (13)$$

where $\sigma = \sigma(\omega_0)$, $\mathcal{D} \equiv \sum_{n \geq 2}^{+\infty} (k^{(n)}/n!) (i\partial_t)^n$ and $T = (1 + \frac{i}{\omega_0} \partial_t)$. The first term of the operator \mathcal{D} corresponds to group-velocity dispersion with coefficient $k'' = \partial^2 k / \partial \omega^2|_{\omega=\omega_0}$. Equation (13) describes wave diffraction, Kerr focusing response, plasma generation, chromatic dispersion with self-consistent deviations from the classical slowly-varying envelope approximation through the space-time focusing and self-steepening operators $[(T^{-1} \nabla_{\perp}^2 \mathcal{E})$ and $(T|\mathcal{E}|^2 \mathcal{E})$, respectively]. This model will be integrated numerically by using initially Gaussian pulses,

$$U(x, y, z = 0, t) = \sqrt{\frac{2P_{in}}{\pi w_0^2}} e^{-\frac{r^2}{w_0^2} - i k_0 \frac{r^2}{2f} - \frac{t^2}{t_p^2}}, \quad (14)$$

which involves the input power P_{in} , the beam waist w_0 and $1/e^2$ pulse half-width t_p . Input pulses can be focused through a lens of focal length f and they linearly diffract over the distance

$$z_f = (f^2/z_0)/(1 + f^2/z_0^2), \quad (15)$$

where $z_0 = \pi n_0 w_0^2 / \lambda_0$ is the Rayleigh range of the collimated beam ($f = +\infty$).

In the coming analysis, we shall employ the nonlinear refractive indices $n_2 = 8 \times 10^{-19}$, 4×10^{-19} , and $1 \times 10^{-19} \text{ cm}^2/\text{W}$ for the wavelengths $\lambda_0 = 248$, 800 and 1550 nm, respectively. At 800 nm, we consider a fitted MPI formulation for the ionization rate, $W(I) \rightarrow \sigma_{(K)} I^K$, where $K = 8$ and $\sigma_{(8)} = 2.88 \times 10^{-99} \text{ s}^{-1} \text{ cm}^{16}/\text{W}^8$. This approximation is known to reproduce experimental data at $\lambda_0 = 800 \text{ nm}$ rather faithfully [28,30]. For the two other wavelengths, we lack well established formulations, so we employ PPT ionization rates. We consider O_2 molecules having the lowest gap potential ($U_i = 12.1 \text{ eV}$) as the main specy undergoing ionization with an effective residual charge $Z_{\text{eff}} = 0.53$ [31]. All ionization rates used in the present paper are illustrated in Fig. 1. They yield saturation intensity below the threshold of $100 \text{ TW}/\text{cm}^2$ currently claimed in the literature [7,11]. The dispersion relation for air has been parametrized as in Ref. [32].

Since our outlook is to understand spectral variations versus the propagation dynamics at different wavelengths, we find it instructive to fix the same ratio of input power over critical, e. g., $P_{in} = 4 \times P_{cr}$, at all wavelengths. To locate the Kerr-driven filamentation onset upon comparable z scales, we also adjust the ratio of the nonlinear focus z_c

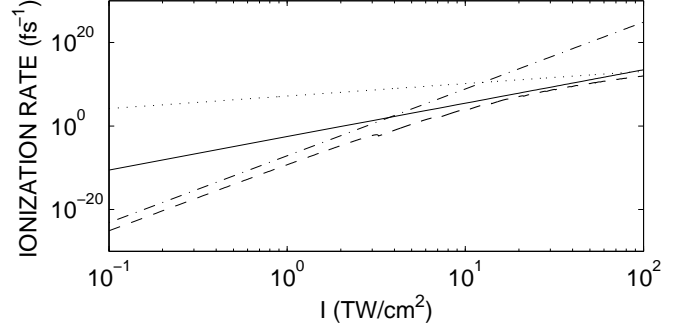


Fig. 1. Ionization rates for the different wavelengths used throughout this paper: $\lambda_0 = 800 \text{ nm}$ (solid line), $\lambda_0 = 248 \text{ nm}$ (dotted line), and $\lambda_0 = 1550 \text{ nm}$ (dashed line). The dashed-dotted line shows the overestimated ionization rate chosen in Sec. 3.2 for $\lambda_0 = 1550 \text{ nm}$.

and Rayleigh range z_0 between 2 and 4, by adapting suitably the beam waist w_0 between 1 and 4 mm.

2.1. Self-phase modulation and SC generation

In air, dispersion is weak with $k'' \lesssim 1 \text{ fs}^2/\text{cm}$ in the UV as well as in the mid-IR domains. Self-channeling then mainly relies on the dynamical balance between Kerr self-focusing and plasma defocusing, so that estimates for peak intensities (I_{max}), electron densities (ρ_{max}) and filament radius (L_{min}) can be deduced from equating diffraction, Kerr and ionization responses in Eq. (13). This yields the simple relations

$$I_{\text{max}} \approx \frac{\rho_{\text{max}}}{2\rho_c n_0 \bar{n}_2}, \quad \rho_{\text{max}} \approx t_p \rho_{nt} W(I_{\text{max}}), \quad (16a)$$

$$L_{\text{min}} \approx \pi (2k_0^2 \bar{n}_2 I_{\text{max}} / n_0)^{-1/2}, \quad (16b)$$

where

$$\bar{n}_2 = n_2 (1 - x_K) + n_2 x_K \max_t \int_{-\infty}^t h(t-t') e^{-2\frac{t'^2}{t_p^2}} dt', \quad (17)$$

represents the maximal effective Kerr index over the initial pulse profile. For practical use, $W(I_{\text{max}})$ can be simplified to $\sigma_K I_{\text{max}}^K$ in MPI-like formulation.

The magnitude of I_{max} directly impacts spectral broadening, which is basically driven by self-phase modulation (SPM). Because the frequency spectrum is expanded by the nonlinearity, SPM leads to SC, as the wave intensity strongly increases through the self-focusing process. Noting by $\varphi(\mathbf{r}, t)$ the phase of the field envelope, frequency variations are dictated in the limit $T, T^{-1} \rightarrow 1$ by

$$\Delta\omega = -\partial_t \varphi \sim -k_0 \Delta z \partial_t (\bar{n}_2 I - \rho / 2n_0 \rho_c), \quad (18)$$

which varies with the superimposed actions of the Kerr and plasma responses. Near the focus point z_c , only the front edge of the pulse survives from this interplay and a redshift is enhanced by plasma generation. At later distances, second focusing/defocusing sequences attenuate this first tendency. In contrast, when accounting for temporal steepening ($T, T^{-1} \neq 1$), shock edges in the back of the pulse are created and a "blue shoulder" appears in the spectrum, to the detriment of the early redshift [7,14,33,34].

In addition, the cubic polarization generates third-order harmonics, modeled by the last term of Eq. (4a). In self-focusing regimes, the third-harmonic intensity usually contributes by a little percentage to the overall beam fluence [16]. Despite its smallness, this component may act as a saturable nonlinearity for the carrier wave. It lowers the peak intensity of the pump and contributes to enhance the blue side of the spectrum after the TH and pump bandwidths increase and overlap [11,13].

3. Long-range Propagation

We numerically analyze supercontinuum generation for the three laser wavelengths of 248 nm, 800 nm and 1550 nm. Results of the nonlinear Schrödinger-like equation (13) for the pump envelope involving or not space-time focusing and self-steepening operators are compared with those of the unidirectional propagation equation (10) avoiding any Taylor expansion in the dispersion relation.

Special attention is here given to the long-range propagation, which rather favors several cycles of focusing-defocusing events. Before proceeding with the above parameters specifically, we perform three different series of simulations showing SC at 800 nm, whose results are summarized in Fig. 2. The first one concerns direct integrations of Eq. (10); the second refers to the same pulse described by Eq. (13), which eludes TH production; the third approach relies on Eq. (13), in which temporal steepening is omitted, i.e., $T = T^{-1} = 1$.

The insets in Fig. 2 show the on-axis spectra when SC is maximal. Following the UPPE description, TH, which emerges from $z_c \sim 6$ m, develops a limited redshift, whereas SC of the fundamental is widely extending towards the blue/UV wavelengths [Fig. 2(a)]. Note that, although a broad plateau occurs in this domain, the TH bandwidth still appears separated from the pump spectrum. Following the NEE description, there is no TH generation. However, SC is so amplified in the blue region by temporal steepening effects, that it overlaps the TH zone and simply hides it [Fig. 2(b)]. Finally, when neglecting temporal steepening, the pump instead develops a wide redshift (overestimated by plasma coupling) and a much narrower blueshift [Fig. 2(c)].

A first observation can be drawn from Fig. 2: Since TH is responsible for lowering the saturation intensity of the pump [13], I_{\max} reached in the UPPE model is lower and the frequency variations $\Delta\omega \sim I_{\max}\Delta z/\Delta t$ are diminished compared with NEE spectra for the pump wave alone. Apart from this difference, no significant other change was detected between both these models, so that NEE seems to be nothing else but the UPPE description subtracted by the self-generated harmonics [7]. Importantly, omitting temporal derivatives of the operators T, T^{-1} imply more serious discrepancies, as can be seen from Fig. 2.

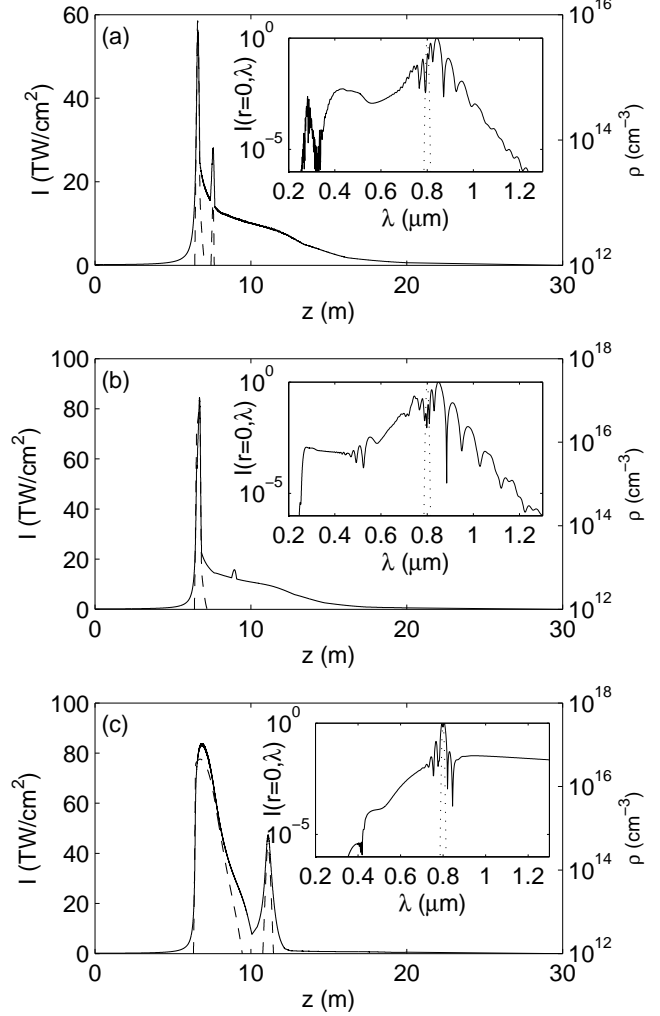


Fig. 2. Peak intensities (solid curves, left-hand side scales) and peak electron densities (dashed curves, right-hand side scales) of 127-fs pulses with ratio of input power over critical equal to 4 and waist $w_0 = 2$ mm at $\lambda_0 = 800$ nm. The insets show on-axis spectra: dotted curves represent the initial spectra; the solid curves the spectra at the propagation distance $z_{\max} = 8$ m where maximal broadening is observed: (a) UPPE model Eq. (10); (b) NEE Eq. (13) applied to the pump wave; (c) NEE Eq. (13) modified with setting $T = T^{-1} = 1$.

3.1. Influence of λ_0

We now examine Gaussian pulses at different wavelengths (248, 800 and 1550 nm) with $t_p = 127$ fs and $P_{\text{in}}/P_{\text{cr}} = 4$ as initial conditions for the UPPE model in parallel geometry ($f = +\infty$). Figures 2(a) and 3 show snapshots of spectra at maximal extent, together with associated peak intensities and electron densities. We here specify that no TH generation was included for $\lambda_0 = 248$ nm, because no reliable data of the dispersion relation was available for this wavelength. We believe, instead, that spectral components below 90 nm should be rapidly absorbed by the medium.

By comparing Figs. 2(a) and 3, it is seen right away that supercontinuum generation increases with the wavelength. To quantify this observation we introduce $\Delta\lambda_{\text{SC}}$ as the to-

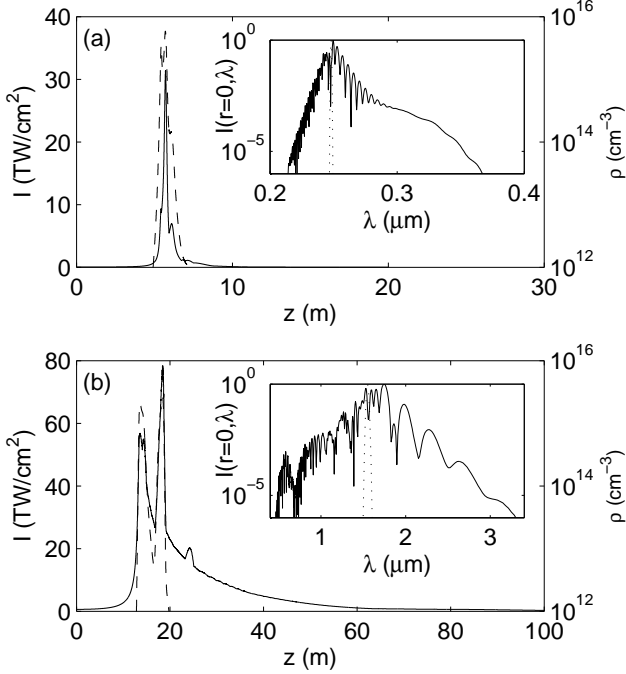


Fig. 3. Peak intensities (solid curves, left-hand side scales) and peak electron densities (dashed curves, right-hand side scales) of 127-fs pulses with ratio of input power over critical equal to 4 at different wavelengths λ_0 . The insets show on-axis spectra: dotted curves represent the initial spectra; the solid curves the spectra at the propagation distance z_{\max} where maximal broadening is observed: (a) $\lambda_0 = 248$ nm, $w_0 = 1$ mm, $z_{\max} = 6$ m; (b) $\lambda_0 = 1550$ nm, $w_0 = 4$ mm, $z_{\max} = 35$ m.

tal extension of the on-axis spectra over wavelengths at 10^{-5} times the maximal spectral intensity. Then a measurement for the effective broadening is the ratio $\Delta\lambda_{SC}/\lambda_0$, which we find close to ~ 0.5 at 248 nm, ~ 1 at 800 nm and ~ 1.5 at 1550 nm. A look at the propagation dynamics reveals that the self-guiding range is noticeably augmented at longer wavelengths. This can be explained by the transverse size of the filament. Equation (16b) gives an estimate for the beam waist in filamentation regime. If we assume comparable I_{\max} for all wavelengths, we deduce that the filament diameter at 1550 nm is about one order of magnitude larger than that at 248 nm, which is compatible with our numerical data. Hence, the larger the wavelength, the slower the filament is expected to diffract. Moreover, by virtue of the formula for the critical power $P_{cr} \propto \lambda_0^2/n_2$ and since a filament conveys a few P_{cr} [7], it is obvious that IR filaments contain much more energy than their UV counterparts. Thus, nonlinear losses along the filamentation range are less dramatic in the IR domain. Due to the longer propagation range, more focusing/defocusing events participate in enlarging the spectra at longer wavelengths. Figure 4 details the evolution of the filaments in the plane (t, z) . It is seen that the time window in which the pulses disperse occupies the length of the input pulse duration. Although shorter temporal peaks arise through self-focusing/defocusing events, multi-peaked profiles mostly develop patterns having a whole extent close to t_p .

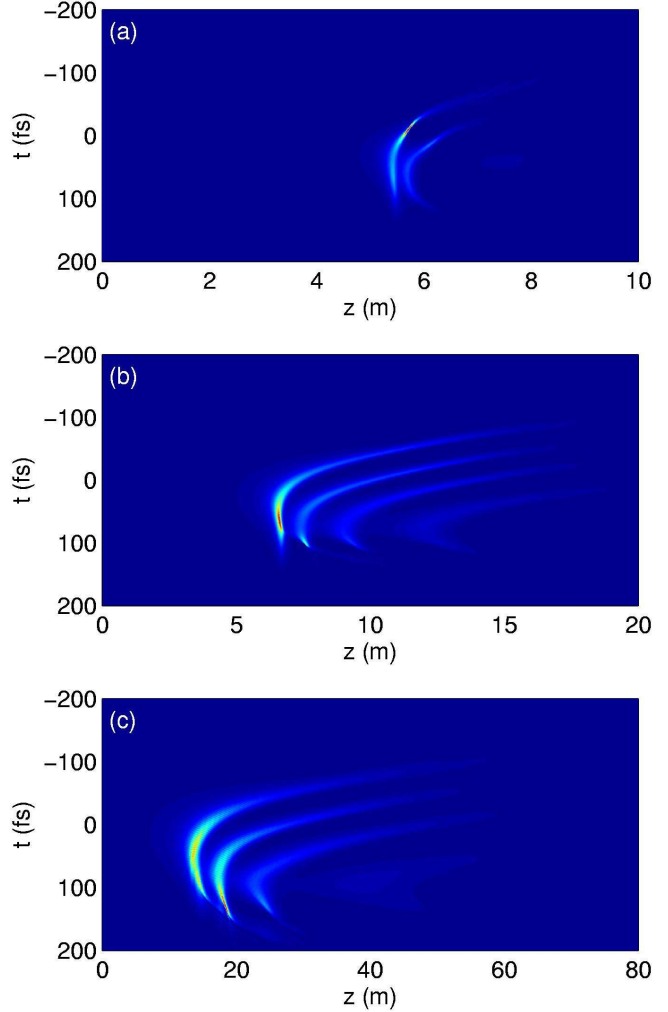


Fig. 4. Temporal evolutions of the pulses shown in Figs. 2(a) and 3 in the (t, z) plane: (a) $\lambda_0 = 248$ nm; (b) $\lambda_0 = 800$ nm; (c) $\lambda_0 = 1550$ nm.

Before going on, we find it worth investigating SC at 1550 nm more thoroughly, in relationship with third-harmonic generation. Figure 5 plots three of the SC development stages, first when TH and pump components are clearly separated ($z = 10$ m), second when they start to merge ($z = 15$ m). At the last propagation distance ($z = 25$ m), we can observe that, unlike Fig. 2, TH and pump spectra overlap and make the TH bandwidth not distinguishable. For comparison, results from the NEE model for the pump wave alone have also been plotted.

3.2. Influence of I_{\max}

The impact of the saturation intensity onto SC is investigated by simply changing the ionization model: By decreasing the photo-ionization rate artificially it is possible to increase I_{\max} and the maximal plasma level ρ_{\max} accordingly. Reversely, increasing $W(I)$ reduces these two quantities, which can have a direct influence on the spectral broadening, as inferred from Eq. (18). To study this point, we concentrate on the wavelength of 1550 nm only,

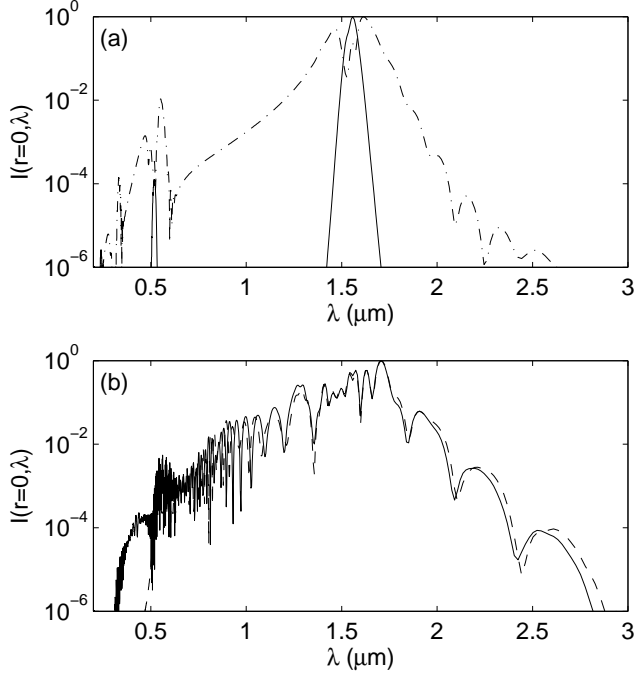


Fig. 5. On-axis spectra for the pulse used in Fig. 3(b) ($\lambda_0 = 1550$ nm) for the propagation distances (a) $z = 10$ m (solid line) and $z = 15$ m (dash-dotted line) and (b) $z = 25$ m (solid line). The dashed line in (b) refers to a spectrum at $z = 25$ m computed from the NEE model.

because it yields the broadest spectra explored so far. Figure 6 shows the maximal intensity and peak electron density at this wavelength, when the ionization rate is artificially increased (see Fig. 1). All other parameters are unchanged, compared with the simulation shown in Fig. 3(b). With the original ionization rate, I_{max} reaches the value of $80 \text{ TW}/\text{cm}^2$; with the artificial one, I_{max} stays below $13 \text{ TW}/\text{cm}^2$. The inset in Fig. 6 details the corresponding spectrum at $z_{\text{max}} = 40$ m. With low I_{max} , the TH component is reduced to some extent as the pump intensity barely exceeds the TH conversion threshold [15]. Meanwhile, SC of the pump driven by the T, T^{-1} operators in the blue side decreases, i.e., a lower I_{max} for analogous pulse compression implies less sharp temporal gradients and smoother optical shocks, which weakens blueshifted frequency variations. These features are visible in Fig. 6, where TH and pump broadbands remain separated. In Figs. 3(b) and 5(b), in contrast, SC extends beyond the TH wavelength and increases more the pulse spectrum. Similar features were observed at the two other wavelengths, when the ionization rate was changed.

3.3. Influence of t_p

We investigate the influence of the initial pulse duration on the propagation dynamics and SC generation. Since we consider transform-limited pulses, the value of t_p is directly linked to the initial spectral width. Moreover, I_{max} comes into play in SC generation and is expected to scale as $\sim (1/t_p)^{1/(K-1)}$ [see Eq. (16a)]. Thus, the initial pulse dura-

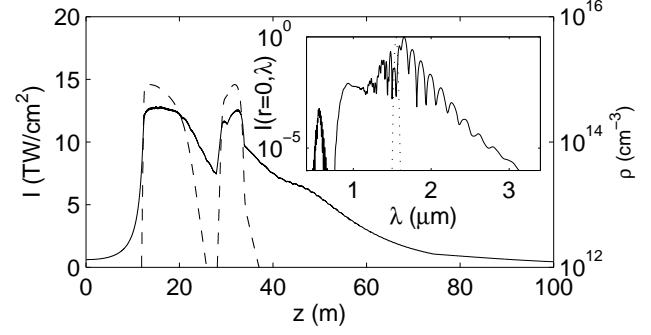


Fig. 6. Peak intensity (solid curve, left-hand side scale) and peak electron density (dashed curve, right-hand side scale) for the same pulse as in Fig. 3(b) ($\lambda_0 = 1550$ nm) computed from the UPPE model with an overestimated ionization rate (see Fig. 1). The inset shows maximal spectral broadening attained at $z_{\text{max}} = 40$ m.

tion should play a significant role in spectral broadening. To check this assessment, we performed several simulations using the UPPE model, by varying t_p from 20 fs up to 500 fs. Because group-velocity dispersion becomes very efficient at short pulse durations and may even stop the Kerr self-focusing at powers too close to critical [35,36], we increased the input power up to $20 P_{\text{cr}}$ for $t_p = 20$ fs. With this, we ensure to trigger a filamentation regime even for this short input duration.

To illustrate the dependency of I_{max} upon t_p , short wavelengths are preferable because the number of photons for ionization is small. Figure 7 shows maximum intensity, peak electron density and maximal spectral extent of a 20-fs pulse at 248 nm. At this wavelength, $K = 3$ and, following Eq. (16a), I_{max} and ρ_{max} should increase by a factor ~ 2.5 compared to the 127-pulse shown in Fig. 3(a). Indeed, both quantities are increased by a factor of ~ 2 in the simulation. Spectral broadening is augmented from 0.5 to 0.8 in terms of $\Delta\lambda_{\text{SC}}/\lambda_0$, especially to the blue side. As explained in Sec. 3.2, this results from the action of the steepening operators. The overall propagation dynamics, characterized by the filamentation length and number of focusing/defocusing cycles are, however, comparable for both the 20-fs and the 127-fs pulses.

On the other hand, if we increase the initial duration t_p towards the ps time scale, the propagation dynamics changes drastically. As an example, Figure 8 shows the temporal evolution of a 500-fs pulse at 800 nm. Compared with Fig. 4(b) employing $t_p = 127$ fs, the obvious difference is the huge number of focusing/defocusing cycles. The action of the generated plasma breaks the pulse profile into a larger number of shorter peaks. With a longer pulse duration, more "time slices" are available for feeding successive focusing events. The filamentation range is increased and I_{max} is maintained over several meters. Inspection of the simulations, however, reveals maximal spectral extent comparable with that displayed in Fig. 2(a).

At 1550 nm the influence of t_p on the maximal intensity is much less pronounced, since we have $K = 15$ [see Figs. 3(b) and 9]. For all pulse durations, we indeed ob-

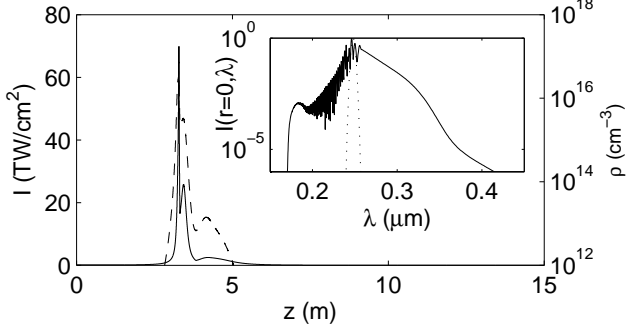


Fig. 7. Peak intensity (solid curve, left-hand side scale) and peak electron density (dashed curve, right-hand side scale) of a 20-fs pulse with ratio of input power over critical equal to 20, $\lambda_0 = 248$ nm, $w_0 = 1$ mm. The inset shows on-axis spectra: the dotted curve represents the initial spectrum; the solid curve the spectrum at the distance $z_{\max} = 3.5$ m where maximal broadening is observed.

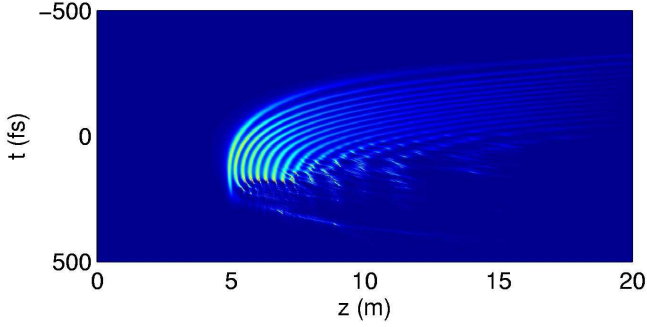


Fig. 8. Temporal evolution of a 500-fs pulse at 800 nm with $4 P_{\text{cr}}$ and waist $w_0 = 2$ mm in the (t, z) plane.

serve $I_{\max} \sim 80$ TW/cm². This can explain why the maximal spectral extension $\Delta\lambda_{\text{SC}}/\lambda_0$ is always found between 1.5 and 2, regardless t_p may be. The major difference lies in the filamentation range, which increases with the initial pulse duration. So, there is no significant change in SC generation between short and long pulses over large enough propagation scales.

This last observation invites us to look at the temporal profiles upon propagation. If the spectral extent is comparable, we might also find similar temporal patterns. Indeed, the on-axis temporal profiles shown in Fig. 10 all exhibit structures with duration of 10-15 fs. It seems that the initial pulse length t_p just determines how many of these peaks appear, or, in other words, how many focusing/defocusing cycles the pulse is able to develop upon propagation. Another indication for the change in the effective pulse duration upon propagation is provided by the curve of the intensity maximum in Fig. 9(b): The first focusing cycle is halted at slightly lower intensities ~ 60 TW/cm², because in this early stage the peak duration remains of the order of $t_p = 500$ fs. At later stages, I_{\max} increases as the pulse undergoes temporal compression.

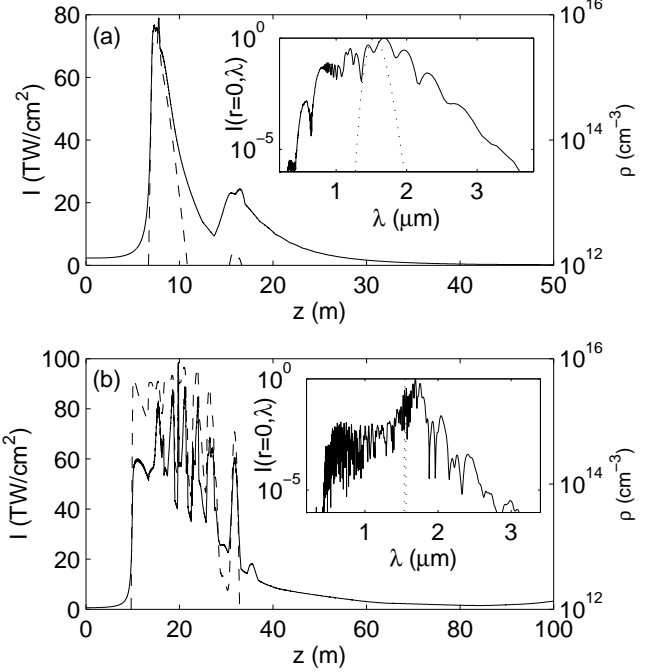


Fig. 9. Peak intensities (solid curves, left-hand side scales) and peak electron densities (dashed curves, right-hand side scales) of 4 mm waisted pulses with different durations and ratios $P_{\text{in}}/P_{\text{cr}}$ at $\lambda_0 = 1550$ nm. The insets show on-axis spectra: dotted curves represent the initial spectra; the solid curves the spectra at the propagation distance z_{\max} where maximal broadening is observed: (a) $t_p = 20$ fs, $P_{\text{in}} = 15 \times P_{\text{cr}}$, $z_{\max} = 20$ m; (b) $t_p = 500$ fs, $P_{\text{in}} = 4 \times P_{\text{cr}}$, $z_{\max} = 40$ m.

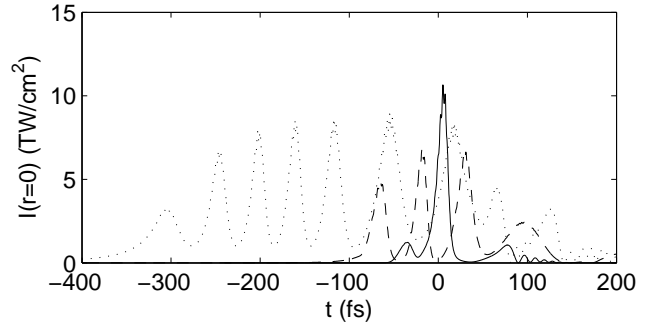


Fig. 10. On-axis temporal profiles of pulses with different duration at z_{\max} : $t_p = 20$ fs [solid line, parameters used in Fig. 9(a)]; $t_p = 127$ fs [dashed line, parameters used in Fig. 3(b)]; $t_p = 500$ fs [dotted line, parameters used in Fig. 9(b)].

4. Short-range Propagation

So far, we have analyzed free propagation dynamics where long filaments achieve temporal gradients and SC extents similar to those produced by initially much shorter pulses. Now, we force all pulses to cover the same short filamentation range through a focusing optics ($f = 2$ m). Results are shown in Fig. 11 for $t_p = 20$ and 500 fs at 1550 nm. We can check that the maximum intensity I_{\max} follows the theoretical expectations (16) involving t_p . The short filamentation range prevents the occurrence of several

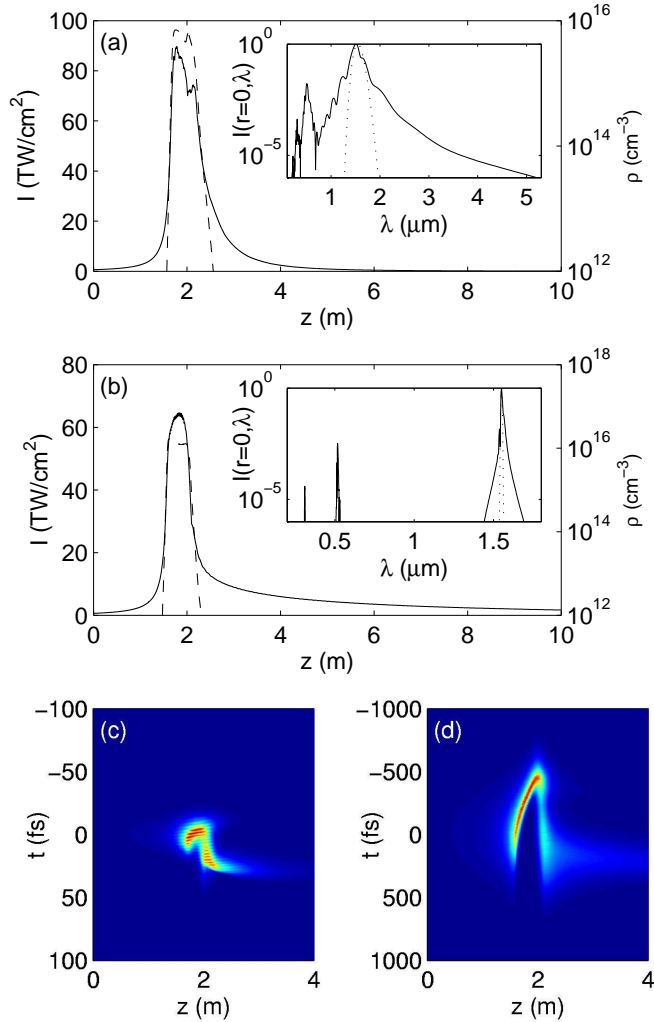


Fig. 11. Peak intensities (solid curves, left-hand side scales) and peak electron densities (dashed curves, right-hand side scales) of 4 mm waisted pulses with different duration and ratio of input power over critical equal to 4 at $\lambda_0 = 1550$ nm propagating in focused geometry ($f = 2$ m). The insets show on-axis spectra: dotted curves represent the initial spectra; the solid curves the spectra at the distance $z_{\max} = 2$ m where maximal broadening is observed: (a) $t_p = 20$ fs; (b) $t_p = 500$ fs. (c) and (d) show the respective temporal evolution for the pulses of (a) and (b) in the (t, z) plane.

focusing/defocusing cycles, especially for the 500-fs pulse. Hence, although the pulse self-focuses, its temporal extent remains comparable with t_p , as we can see in Figs. 11(c) and (d). The 20-fs pulse shows significant spectral broadening with a visible, broadened TH peak. The 500-fs pulse is spectrally too narrow to generate supercontinuum over roughly 1-m filamentation range. Therefore, the fundamental and harmonic peaks clearly stay separated (note the occurrence of the fifth harmonics at 310 nm, which is self-consistently described by the UPPE model). Thus, the initial pulse duration strongly influences spectral broadening in configurations of short filamentation range mainly, which is consistent with the numerical results of Ref. [21].

5. Conclusion

In summary, we have revisited recent works on SC generation versus third harmonic emission, by showing from a complete UPPE model that spectral enlargements of femtosecond pulses in self-guiding regime are mostly driven by space-time focusing and self-steepening. TH generation, although changing the pump dynamics, affects the spectra to a limited extent only. This conclusion corrects some previous statements [19], based on a propagation model in which temporal steepening terms were analyzed separately from an envelope description for TH generation. Going one step beyond, we have demonstrated the important role of the saturation intensity in the frequency variations enlarging both TH and pump broadbands. The input pulse duration becomes a significant player in the spectral extents as long as pulses do not propagate too far, i.e., they do not let the temporal profiles of the pulse fluctuate so much that many peaks and sharp gradients can develop along the optical path. This property is mainly enlightened in short-range focused geometry and lost in long-range parallel geometry. Finally, the role of the central wavelength is preeminent: Our numerical simulations displayed evidence that SC clearly augments with the laser wavelength.

References

- [1] R. R. Alfano (Ed.), *The Supercontinuum Laser Source*, Springer-Verlag, Germany, 1989.
- [2] S. L. Chin, A. Brodeur, S. Petit, O. G. Kosareva, V. P. Kandidov, Filamentation and supercontinuum generation during the propagation of powerful ultrashort laser pulses in optical media (white light laser), *J. Nonlinear Opt. Phys. Mater.* 8 (1999) 121.
- [3] S. Backus, J. Peatross, Z. Zeek, A. Rundquist, G. Taft, M. M. Murnane, H. C. Kapteyn, 16-fs, 1-μJ ultraviolet pulses generated by third-harmonic conversion in air, *Opt. Lett.* 21 (1996) 665.
- [4] A. B. Fedotov, N. I. Koroteev, M. M. T. Loy, X. Xiao, A. M. Zheltikov, Saturation of third-harmonic generation in a plasma of self-induced optical breakdown due to the self-action of 80-fs light pulses, *Opt. Commun.* 133 (1997) 587.
- [5] G. Marcus, A. Ziegler, Z. Henis, Third-harmonic generation at atmospheric pressure in methane by use of intense femtosecond pulses in the tight-focusing limit, *J. Opt. Soc. Am. B* 26 (1999) 791.
- [6] J. Kasparian, M. Rodriguez, G. Méjean, J. Yu, E. Salmon, H. Wille, R. Bourayou, S. Frey, Y. B. André, A. Mysyrowicz, R. Sauerbrey, J. P. Wolf, L. Wöste, White-light filaments for atmospheric analysis, *Science* 301 (2003) 61.
- [7] L. Bergé, S. Skupin, R. Nuter, J. Kasparian, J. P. Wolf, Optical ultrashort filaments in weakly-ionized, optically-transparent media, <http://arxiv.org/abs/physics/0612063>, submitted to *Rev. Mod. Phys.* (2006).
- [8] V. I. Bespalov, V. I. Talanov, Filamentary structure of light beams in nonlinear liquids, *JETP Lett.* 3 (1966) 307.
- [9] M. Mlejnek, M. Kolesik, J. V. Moloney, E. M. Wright, Optically turbulent femtosecond light guide in air, *Phys. Rev. Lett.* 83 (1999) 2938.
- [10] S. L. Chin, S. Petit, W. Liu, A. Iwasaki, M.-C. Nadeau, V. P. Kandidov, O. G. Kosareva, K. Y. Andrianov, Interference of

- transverse rings in multifilamentation of powerful femtosecond laser pulses in air, *Opt. Commun.* 210 (2002) 329.
- [11] N. Aközbek, A. Becker, M. Scalora, S. L. Chin, C. M. Bowden, Continuum generation of the third-harmonic pulse generated by an intense femtosecond IR laser pulse in air, *Appl. Phys. B: Lasers & Optics* 77 (2003) 177.
 - [12] F. Théberge, W. Liu, Q. Luo, S. L. Chin, Ultrabroadband continuum generated in air (down to 230 nm) using ultrashort and intense laser pulses, *Appl. Phys. B: Lasers & Optics* 80 (2005) 221.
 - [13] L. Bergé, S. Skupin, G. Méjean, J. Kasparian, J. Yu, S. Frey, E. Salmon, J. P. Wolf, Supercontinuum emission and enhanced self-guiding of infrared femtosecond filaments sustained by third-harmonic generation in air, *Phys. Rev. E* 71 (2005) 016602.
 - [14] N. Aközbek, M. Scalora, C. M. Bowden, S. L. Chin, White-light continuum generation and filamentation during the propagation of ultra-short laser pulses in air, *Opt. Commun.* 191 (2001) 353.
 - [15] H. Yang, J. Zhang, J. Zhang, L. Z. Zhao, Y. J. Li, H. Teng, Y. T. Li, Z. H. Wang, Z. L. Chen, Z. Y. Wei, J. X. Ma, W. Yu, Z. M. Sheng, Third-order harmonic generation by self-guided femtosecond pulses in air, *Phys. Rev. E* 67 (2003) 015401(R).
 - [16] N. Aközbek, A. Iwasaki, A. Becker, M. Scalora, S. L. Chin, C. M. Bowden, Third-harmonic generation and self-channeling in air using high-power femtosecond laser pulses, *Phys. Rev. Lett.* 89 (2002) 143901.
 - [17] I. Alexeev, A. C. Ting, D. F. Gordon, E. Briscoe, B. Hafizi, P. Sprangle, Characterization of the third-harmonic radiation generated by intense laser self-formed filaments in air, *Opt. Lett.* 30 (2005) 1503.
 - [18] F. Théberge, N. Aközbek, W. Liu, J.-F. Gravel, S. L. Chin, Third harmonic beam profile generated in atmospheric air using femtosecond laser pulses, *Opt. Commun.* 245 (2005) 399.
 - [19] G. Méjean, J. Kasparian, J. Yu, S. Frey, E. Salmon, R. Ackermann, J.-P. Wolf, L. Bergé, S. Skupin, UV-supercontinuum generated by femtosecond pulse filamentation in air: Meter-range experiments versus numerical simulations, *Appl. Phys. B: Lasers & Optics* 82 (2006) 341.
 - [20] S. A. Trushin, S. Panja, K. Kosma, W. E. Schmid, W. Fuss, Supercontinuum extending from > 1000 to 250 nm, generated by focusing ten-fs laser pulses at 805 nm into Ar, *Appl. Phys. B: Lasers & Optics* 80 (2005) 399.
 - [21] N. Aközbek, S. A. Trushin, A. Baltuška, W. Fuss, E. Goulielmakis, K. Kosma, F. Krausz, S. Panja, M. Uiberacker, W. E. Schmid, A. Becker, M. Scalora, M. Bloemer, Extending the supercontinuum spectrum down to 200 nm with few-cycle pulses, *New J. Phys.* 8 (2006) 177.
 - [22] M. Kolesik, E. M. Wright, A. Becker, J. V. Moloney, Simulation of third-harmonic and supercontinuum generation for femtosecond pulses in air, *Appl. Phys. B: Lasers & Optics* 85 (2006) 531.
 - [23] M. Kolesik, J. V. Moloney, M. Mlejnek, Unidirectional optical pulse propagation equation, *Phys. Rev. Lett.* 89 (2002) 283902.
 - [24] J. R. Peñano, P. Sprangle, P. Serafim, B. Hafizi, A. Ting, Stimulated raman scattering of intense laser pulses in air, *Phys. Rev. E* 68 (2003) 056502.
 - [25] P. Sprangle, J. R. Peñano, B. Hafizi, Propagation of intense short laser pulses in the atmosphere, *Phys. Rev. E* 66 (2002) 046418.
 - [26] A. M. Perelomov, V. S. Popov, M. V. Terent'ev, Ionization of atoms in an alternating electric field: II, *Sov. Phys. JETP* 24 (1967) 207.
 - [27] M. V. Ammosov, N. B. Delone, V. P. Krainov, Tunnel ionization of complex atoms and of atomic ions in an alternating electromagnetic field, *Sov. Phys. JETP* 64 (1986) 1191.
 - [28] R. Nuter, L. Bergé, Pulse chirping and ionization of O_2 molecules for the filamentation of femtosecond laser pulses in air, *J. Opt. Soc. Am. B* 23 (2006) 874.
 - [29] T. Brabec, F. Krausz, Nonlinear optical pulse propagation in the single-cycle regime, *Phys. Rev. Lett.* 78 (1997) 3282.
 - [30] S. Skupin, L. Bergé, U. Peschel, F. Lederer, G. Méjean, J. Yu, J. Kasparian, E. Salmon, J.-P. Wolf, M. Rodriguez, L. Wöste, R. Bourayou, R. Sauerbrey, Filamentation of femtosecond light pulses in the air: Turbulent cells versus long-range clusters, *Phys. Rev. E* 70 (2004) 046602.
 - [31] A. Talebpour, J. Yang, S. L. Chin, Semi-empirical model for the rate of tunnel ionization of N_2 and O_2 molecule in an intense Ti:sapphire laser pulse, *Opt. Commun.* 163 (1999) 29.
 - [32] E. R. Peck, K. Reeder, Dispersion of air, *J. Opt. Soc. Am.* 62 (1972) 958.
 - [33] J. E. Rothenberg, Pulse splitting during self-focusing in normally dispersive media, *Opt. Lett.* 17 (1992) 584.
 - [34] G. Yang, Y. R. Shen, Spectral broadening of ultrashort pulses in a nonlinear medium, *Opt. Lett.* 9 (1984) 510.
 - [35] S. Skupin, L. Bergé, Self-guiding of femtosecond light pulses in condensed media: Plasma generation versus chromatic dispersion, *Physica D* 220 (2006) 14.
 - [36] S. Skupin, R. Nuter, L. Bergé, Optical femtosecond filaments in condensed media, *Phys. Rev. A* 74 (2006) 043813.